



## Research paper

Coupling of multi-vibrational modes in bacteriochlorophyll *a* in solution observed with 2D electronic spectroscopy

Shuai Yue, Zhuan Wang, Xuan Leng, Rui-Dan Zhu, Hai-Long Chen, Yu-Xiang Weng\*

Beijing National Laboratory for Condensed Matter Physics, CAS Key Laboratory of Soft Matter Physics, Institute of Physics, Chinese Academy of Sciences, Beijing 100190, China  
University of Chinese Academy of Sciences, Beijing 100049, China

## ARTICLE INFO

## Article history:

Received 4 December 2016  
In final form 10 March 2017  
Available online 11 March 2017

## Keywords:

2DES  
BChla  
B820  
Coherence  
Wave-packet

## ABSTRACT

Low vibrational modes in a range of 80–400  $\text{cm}^{-1}$  for bacteriochlorophyll *a* are excited and observed as beating dynamics in two-dimensional electronic spectra. A coupled multi-vibrational mode displaced oscillator model is proposed to account for the vibronic coherence. We found that these low frequency vibrational modes are coupled. By comparing the fitted lifetime of the vibrational modes appearing in the beating dynamics for bacteriochlorophyll *a* and a protein-bound bacteriochlorophyll *a* dimer B820 probed by transient grating method, it is suggested that the protein scaffold provides a protection effect on the vibronic coherence where no excitonic coherence has been excited.

© 2017 Elsevier B.V. All rights reserved.

## 1. Introduction

Photosynthesis is a fundamental biological process converting solar energy into organic substances in large scale. The primary process in photosynthesis involves several elementary steps including light-harvesting, energy transfer and charge separation proceeding on the photosynthetic machinery such as light harvesting antenna complexes and the reaction centers (RCs). The construction of the machinery uses only a few kinds of pigment molecules bound to the proteins. One important strategy of tuning the spectral region of light absorption in the antenna complexes is to use the aggregated pigment molecules in either homo- or hetero forms. Among which bacteriochlorophyll *a* (BChla) is such a key construction pigment molecule found in many photosynthetic bacteria, e.g., in Fenna-Matthewa-Olson (FMO) the antenna complex and the dimer form in the RC. It has been found that the energy transfer efficiency in the primary photosynthetic processes can be as high as 95–100% [1]. In account for such a high energy transfer efficiency, in addition to the incoherent Förster energy transfer mechanism, a novel mechanism with spatially delocalized excitons has also been proposed which involves a wave-like energy transfer pathway [2]. Excitation of the delocalized excitons in the aggregated pigment molecules creates a superposition of the electronic states, which would lead to the quantum coherence (quantum beat) in the subsequent dynamics. In experiment, coherent nuclear

motion in biological samples on picosecond time scale were first reported in the pump-probe studies of the photosynthetic bacterial RC associated with photoinduced electron transfer by Vos et al. [3,4]. Later Engel et al. reported oscillations in the two-dimensional spectra of the FMO complex of BChla with two-dimensional electronic spectroscopy (2DES) [5] which has an enhanced spectral selectivity beyond that achieved by many other femtosecond optical techniques such as pump-probe or transient grating (TG), by spreading the spectral contents over two independent frequency axes at a given delay time [6]. Furthermore, the cross peaks in 2DES contain information about the electronic coherence. By use of the 2DES, sustained beating between optically excited states in photosynthetic protein complexes lasting several hundred femtoseconds at room temperature, and up to nearly 2 picoseconds in FMO complex at 77 K have been observed. The observed oscillations survive over a picosecond and were ascribed to beating between delocalized excitonic (electronic) states [5,7]. After then, oscillatory dynamics at early population time in photosynthetic protein complexes other than FMO including the antenna and reaction centers (RCs) even at room temperature have been observed with 2DES [8–15]. Furthermore, coherence phenomenon among a number oscillating frequencies ranging from 91 to 974  $\text{cm}^{-1}$  has been observed for chlorophyll *a* dimer in PS II RCs. The coherence was interpreted in a model of single vibration mode coupled to several excitonic levels [16].

These experiments have inspired discussion on what role coherence could play in the energy and electron transfer [14]. However, this observation also triggered a debate about the nature of the

\* Corresponding author.

E-mail address: [yxweng@aphy.iphy.ac.cn](mailto:yxweng@aphy.iphy.ac.cn) (Y.-X. Weng).

oscillation, i.e., it is of electronic, vibronic or vibrational coherence, in the two folds: (1) the observed long-lasting oscillation time well exceeds the theoretically simulated value for the electronic coherence of 200–300 fs at room temperature [17]; (2) the interpretation of the 2DES is complicated which relies heavily on the model proposed. Therefore, it is still challenging for 2DES to distinguish signatures of coherent molecular vibrations from coherent superposition of electronic states [11,14,18–20]. Recent coherent multidimensional spectroscopic studies of the nature of the quantum coherence in antennas and RCs have shown that the long-lived coherence can arise from a mixed electronic-vibronic state [11,19]. Detailed analysis of the dynamics of these types of model systems has revealed that the strong coupling of the vibrational mode to the electronic states can lead to a dephasing time longer than that expected for the quantum superposition of bare excitonic levels [11,21–24].

The experimental findings and subsequent theoretical studies have led to the speculation that coherent energy transfer may be relevant for photosynthesis *in vivo*, that the exciton–phonon interaction allows for energy to flow in a wave-like manner in the biological environment [19,25]. This apparently involves the low vibration modes either from the protein environment or the chromophores themselves [12], where the protein fluctuations can generate non-equilibrium processes that lead to the spontaneous creation and sustenance of electronic coherence, even at physiological temperatures [21]. While others suggested that the protein creates a local environment protecting chromophores and coherences from external environmental fluctuations [6,26]. When vibrational modes of the chromophores are considered, the long-lived vibronic coherences are found to be generated only when the frequency of the mode is in the vicinity of [24] or in resonance with the electronic energy difference [12], since the time-resolved measurements have shown that low frequency vibrational coherences in BChls have a dephasing time on the order of a few picosecond [27]. Generally, the electronic energy difference is much larger than the low frequencies of the vibrational modes as well as those of the proteins environment, and how the high frequencies of the vibronic states in resonance with the electronic energy splitting are coupled to the low vibrational frequencies of the chromophores and proteins are still unclear. Resonance Raman (RR) spectra obtained from reaction centers with isotopically labeled cofactors and normal-coordinate analyses suggest that intramolecular BChla modes are involved [28,29]. Several of these modes have an out-of-plane character that would modulate the strong electronic coupling and intramolecular charge transfer properties of the special pair [30,31]. Earlier attempts to observe underdamped vibrational coherence from monomeric BChla in pyridine by using 50 fs laser in pump-probe were unsuccessful [32,33]. Later Shelly et al. observed the low frequency coherence with more than 10 modes in a spectral region of 10–220  $\text{cm}^{-1}$  with the same method [27]. Furthermore, Fransted et al. investigated the vibrational coherence in 2D spectra for BChla monomer in solutions, only a few higher vibrational modes ( $>500 \text{ cm}^{-1}$ ) were observed [34].

In this letter, we revisited the 2DES of the low vibrational modes of the BChla monomer in ethanol solution based on the reported displaced oscillator model [20] with further incorporation of coupling among the multiple vibrational modes. The oscillation arising from the vibrational coherence were analyzed in 2D frequency map constructed by Fourier transformation along the population waiting time, and the amplitude of the observed beating frequency is represented, which has a higher selectivity than the 2D spectra [35]. We found that several low frequency vibrational modes within 80–400  $\text{cm}^{-1}$  are coupled.

## 2. Experimental

### 2.1. Sample preparation

BChla was used as received from Sigma-Aldrich and dissolved in ethanol at a concentration of 0.1 mM. The B820 subunit of light harvesting antenna complex LH1 in the presence of 1% (w/v) *n*-octyl  $\beta$ -D-glucopyranoside ( $\beta$ -OG, Aldrich) was isolated from the chromatophores of *Rhodospirillum rubrum* G9 bacteria as described by Miller et al. [36]. All of the solvents were of analytical grade. The samples were recycled by peristaltic pump at a rate of about 0.1 m/s during the measurement. The optical density (OD) of B820 was adjusted to 0.1/mm for the 2DES and TG measurements. The absorption and fluorescence spectra of BChla and B820 were measured on HITACHI U-3010 absorption spectrophotometer and HITACHI F-4500 fluorescence spectrophotometer respectively.

### 2.2. Apparatus for 2DES and TG

The spectrometer for 2DES used in these experiments follows the traditional version of the diffractive optics reported by Brixner et al. [37], and have been described in detail elsewhere [38]. Briefly, a commercial Ti:sapphire laser (Spitfire Ace, Spectra Physics) with a pulse width of 35 fs, working at a repetition rate of 500 Hz, and a central output wavelength at 800 nm with approximately 30 nm spectral width was used as the light source for the implementation of 2DES. To achieve a broader spectral range, white-light filament generated by focusing 800 nm beam onto the air by a convex lens with a focal length of 1 m was split into four beams used in 2DES. The spectrum of the white-light filament is shown in Fig. 1. During the experiment, the intensity of the first three pulses at a focal point size of 130  $\mu\text{m}$  (FWHM) were adjusted to 40 nJ/pulse, and that of the local oscillator beam was attenuated to 40 pJ/pulse. The instrumental response time was evaluated by the optical induced Kerr effect of ethanol, which is less than 50 fs (see Supporting Information (SI) Fig. S1). The shot-to-shot fluctuation of the output laser intensity was kept lower than 0.5%. As a result, the phase stability of the 2DES can be achieved with a typical value of  $\lambda/90$  at 800 nm. Coherence time region was scanned between  $\pm 135$  fs in 0.533 fs time interval. Population delay time was scanned with a step of 10 fs, the data points in the first 80 fs were discarded owing to the possible artifact from the interference of

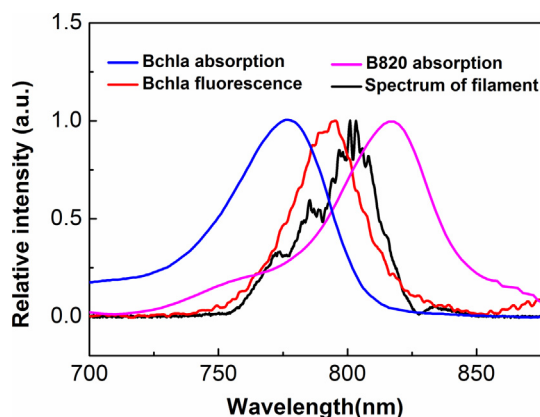


Fig. 1. Absorption spectrum (blue) and fluorescence spectrum (red) with an excitation wavelength at 785 nm of BChla in ethanol; the absorption spectrum of B820 (magenta) and the spectrum of the white-light filament beam (black) used in the experiment. (For interpretation of the references to colour in this figure legend, the reader is referred to the web version of this article.)

the two pump beams [34]. The temporal range of data for Fourier transformation was up to 500 fs having 51 data points, which was zero-padded to 500 units, corresponding to a total time window of 5 ps, and no window function was used, which leads to an estimated spectral resolution around 21–36  $\text{cm}^{-1}$  for the vibrational mode detected from the beating dynamics with aid of the secondary derivative analysis of the beating frequency spectrum probed at a certain given wavelength. Such an estimation is based on the following procedure: From the temporal scanning range of 500 fs in the waiting time, the spectral resolution for the low frequency beating modes can be calculated to be 67  $\text{cm}^{-1}$ . Zero-padding method in Fourier transformation would further improve this spectral resolution to less than 67  $\text{cm}^{-1}$ . For vibrational peaks, their line shapes can generally be simulated by Gaussian or Lorentzian function. In the current case, we assume that all the peaks can be fitted by Gaussian form. For a perfect Gaussian form, the spectral resolution can be enhanced by a factor of 1.88 when taking its secondary derivative. Thus the spectral resolution after secondary derivative analysis can be further improved to an upper limit of less than 36  $\text{cm}^{-1}$ . The lower limit is derived from the narrowest peak found in the secondary derivative spectra, which has a full-width-at-half-measure of 21  $\text{cm}^{-1}$  (only the negative peaks in the second derivative spectra can be used for analysis). The measured 2DES for BChla at two typical population delay time are provided in SI Fig. S2. TG experiment was conducted on the same device with the local oscillator beam being blocked, and the coherence time delay set to zero. The population delay time was scanned

up to 3 ps with a time interval of 6.66 fs, corresponding to a frequency resolution about 10  $\text{cm}^{-1}$ .

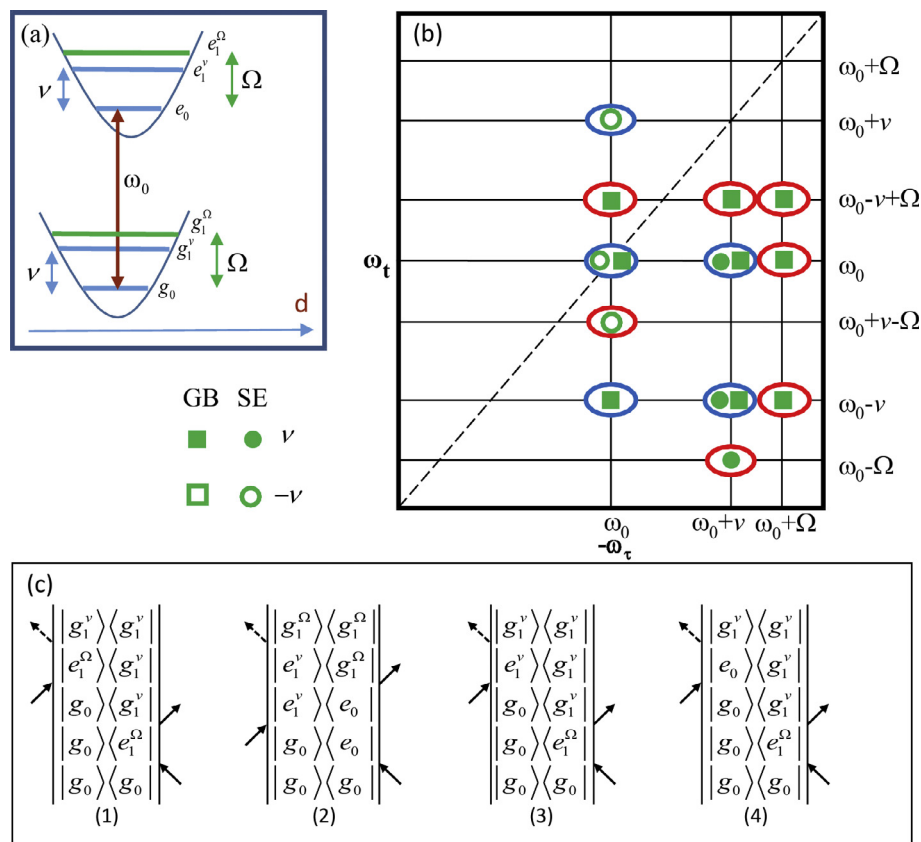
### 3. Results and discussion

Fig. 1 shows the absorption spectra of BChla in ethanol and B820 solution, as well as the corresponding fluorescence spectrum of BChla and the spectrum of the white-light filament.

For BChla, the peak position of  $Q_x$  absorption can be used to identify the coordination state of  $\text{Mg}^{2+}$ , i.e., when the absorption appears at 580 nm, it indicates that the  $\text{Mg}^{2+}$  ion is five-coordinated, with one solvent molecule as the ligand bound to an axial site; whereas that of 600 nm indicates that the  $\text{Mg}^{2+}$  ion is six-coordinated, with two solvent molecule bound to each of the axial sites [27]. The  $Q_x$  of BChla in ethanol is at 597 nm and that of B820 at 594 nm (data not shown), indicating both the BChla in ethanol or in B820 being six-coordinated.

In the current work, beating dynamics were observed in BChla along the population delay time ( $T$ ), which can be more conveniently characterized in terms of oscillation Fourier maps (also known as 2D frequency map [35]) as a slice of a 3DES constructed by applying the Fourier transformation to the real part of the rephasing spectrum  $S_R(\omega_t, T, \omega_\tau)$  with respect to the population delay time  $T$  [6,10,20,35,39]

$$A(\omega_t, \omega_T, \omega_\tau) = \int_0^\infty dT e^{i\omega T} \text{Re} S_R(\omega_t, T, \omega_\tau). \quad (1)$$



**Fig. 2.** (a) Multi-vibrational mode-coupled displaced oscillator model with electronic transition energy  $\omega_0$  and two vibrational modes having a specific transition frequency of  $\nu$  and  $\Omega$  respectively; (b) Cartoon rephasing Fourier map for the vibrational mode-coupled displaced model at the oscillation frequency  $\omega_\tau = \nu$ , displaying the uncoupled pattern (blue ellipses) and the two vibrational mode coupled pattern (red ellipses). The squares represent the beating appearing in the ground-state bleaching (GB) signals while the circles in the stimulated emission (SE) signals. The filled symbols for the beating with  $+\nu$  frequency while the open ones for the  $-\nu$  frequency. (c) Feynman diagrams of four typical coupling cases having a beating frequency of  $\pm\nu$ . The subscript indicates ladder of the mode, and the superscript indicates the vibrational mode. (For interpretation of the references to colour in this figure legend, the reader is referred to the web version of this article.)

The Fourier maps for displaced oscillator, electronic dimer [20] or system eigenstates [40] have been presented previously. In contrast, we present the Fourier map based on a multi-vibrational mode coupled displaced oscillator with an electronic transition energy  $E(\omega_0)$  and two normal vibrational normal modes of different frequency  $\nu$  and  $\Omega$  ( $\Omega > \nu$ ) respectively, as a simplified model for the coupling of multi-vibrational mode during the electronic transition.

A brief theoretical account for the multimode coupling in 2DES is given as follows. For a single vibrational mode displaced oscillator coupled to the electronic states of a chromophore molecule, the Hamiltonian as well as the corresponding sets of wave functions have been given by Butkus et al. [41,42]. In the current work, we need to extend the single mode case to the multi-mode case. Following the work of Fidler and Engel [43], for a multi-mode coupled displaced oscillator, we consider a chromophore molecule with only two electronic states, i.e., the ground state  $|g\rangle$  and the excited state  $|e\rangle$ , coupled to a collection of harmonic oscillators within the adiabatic approximation. The total Hamiltonian can be expressed as

$$H = H_g|g\rangle\langle g| + H_e|e\rangle\langle e| \quad (2)$$

where

$$H_g = \sum_i \left( \frac{p_i^2}{2\mu_{gi}} + \frac{1}{2}\mu_{gi}\omega_{gi}^2 q_i^2 \right) \quad (3)$$

$$H_e = h\omega_{eg} + \sum_i \left( \frac{p_i^2}{2\mu_{gi}} + \frac{1}{2}\mu_{ei}\omega_{ei}^2 (q_i - d_i)^2 \right) \quad (4)$$

Here  $i$  represents the  $i$ th vibrational mode,  $p_i$  and  $q_i$  are the corresponding momentum and the position operator respectively.  $\mu_{gi}$  ( $\mu_{ei}$ ) is the reduced mass of the ground (excited) state,  $\omega_{gi}$  ( $\omega_{ei}$ ) is the frequency of the oscillator on the ground (excited) state,  $d_i$  is the displacement of the origin on the excited-state potential relative to the ground state along the coordinate  $q_i$ , and  $\omega_{eg}$  is the energy difference between the minima of the two electronic states. An assumption is made that the nuclear potential surfaces are well described as harmonic and that the excited energy surface is

allowed to differ in curvature, giving rise to that the values of  $\omega_{ei}$  and  $\omega_{gi}$  can be different.

The schematic diagram for the coupled two normal mode displaced oscillator model is shown in Fig. 2(a), the expected Fourier map for a given oscillation frequency  $\nu$  with a coupled mode  $\Omega$  is in Fig. 2(b) and the corresponding four Feynman diagrams leading to the mode coupling in Fig. 2(c) (For complete sets of Feynman diagrams see SI Fig. S3). It has been shown that in the displaced oscillator model containing a single vibrational mode, the beating oscillation frequency denoted as  $\nu$  appears at the rephasing frequency in the Fourier map at  $\omega_0 - \nu$ ,  $\omega_0$ ,  $\omega_0 + \nu$ , representing the ground-state coherence, mixed-state coherence and the excited state coherence respectively [12], leading to a ‘chair’ pattern [35] as indicated by the blue ellipses in Fig. 2(b). In contrast, the two vibrational mode coupled displaced oscillator model shows that, except for the uncoupled single mode pattern, the coupled pattern appears at the location of the rephasing frequency at  $\omega_0 - \nu + \Omega$  excited at  $\omega_0$ ,  $\omega_0 + \nu$  and  $\omega_0 + \Omega$ ; rephasing frequency at  $\omega_0 + \nu - \Omega$  excited at  $\omega_0$ ; rephasing frequency at  $\omega_0 - \nu$  excited at  $\omega_0 + \Omega$ ; rephasing frequency at  $\omega_0 - \Omega$  excited at  $\omega_0 + \nu$ . These indicate that the observed beating frequency  $\nu$  can be excited at a vibrational frequency corresponding either to  $\omega_0 + \nu$  or to  $\omega_0 + \Omega$ . The fact suggests that the vibrational frequencies  $\nu$  and  $\Omega$  are coupled to each other.

Fig. 3 presents the experimentally observed Fourier map for a typical beating frequency of  $\omega_T = 200 \text{ cm}^{-1}$  where the ‘chair’ pattern of uncoupled beating locations are labeled in blue and the coupled ones are in red in accordance with Fig. 2(b). The circles stand for those determined locations with help of the secondary derivative analysis. Two coupled vibrational modes with frequencies of 80 and  $440 \text{ cm}^{-1}$  were resolved. While the rephasing and non-rephasing Fourier maps for the other observed beating frequencies with  $\omega_T = 80, 160, 200, 280, 340$  and  $400 \text{ cm}^{-1}$  are provided in SI Figs. S4 and S5. The coupling of the given beating frequency to the others read from the corresponding Fourier maps are summarized in Table 1, which shows that coupling of one beating mode to a number of other modes have been observed. Owing to the broad bandwidth along the excitation frequency, only part of the coupling locations can be determined, while the cross points of the white lines in Fig. 3(a) indicates the expected locations of mode

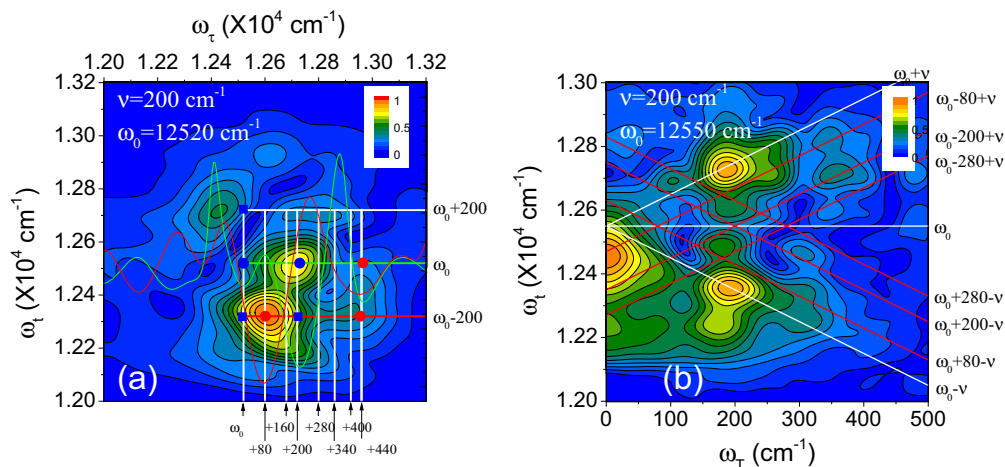


**Fig. 3.** (a) Rephasing Fourier map for a typical beating frequency of  $\omega_T = 200 \text{ cm}^{-1}$  derived from the 3DES. Locations of these beating frequencies are classified as the uncoupled group (blue color, chair pattern) and the group coupled to the other vibrational modes (red color,  $\Omega = 80, 160, 280$  and  $340 \text{ cm}^{-1}$ ) according to Fig. 2(b); the squares stand for the expected locations, while the filled circles stand for those determined by means of secondary derivative of the projected curves along the horizontal lines (downward negative peaks). The red curve is the secondary derivative of the beating frequency spectrum projected along  $\omega_t = \omega_0 - 200$  (red line) and the green curve is that along  $\omega_t = \omega_0$  (green line). (b) Power spectrum for the beating frequency derived as a slice through the rephasing frequency  $\omega_t$  from the 3DES at a given excitation frequency as indicated near the (0–0) transition energy [12]. The pair of white lines indicate the uncoupled vibrational peaks defined as  $\omega_0 \pm \nu$ ; whereas the pairs of lines in red color represent the expected coupled vibrational peak locations defined as  $\omega_0 \pm \omega_T \mp \Omega$ , with  $\Omega = 80, 200$  and  $280 \text{ cm}^{-1}$  respectively, where  $\pm\Omega$  can be read from the intercepts.

**Table 1**

Observed beating frequencies together with their corresponding coupled vibrational frequencies resolved by rephasing Fourier maps.

Beating frequency (cm <sup>-1</sup> )	Observed coupled vibrational frequencies in Fourier map (cm <sup>-1</sup> )						
	80	160	200	280	340	400	440
80			✓	✓			
160	✓		✓	✓			✓
200	✓						✓
280	✓	✓	✓		✓		✓
340	✓	✓	✓	✓		✓	
400	✓	✓	✓	✓	✓		

coupling. It should be noted that these beating frequencies can find their corresponding counterpart in RR spectrum [28].

The coupling of the a single beating frequency to the other vibrational modes can be viewed more straight-forwardly in another representation of rephasing power spectrum [12] for the beating frequency  $\omega_T$  at a given excitation frequency as shown in Fig. 3(b), i.e., in equation (1) by fixing the excitation frequency as  $\omega_\tau = \omega_0$ , one has  $A(\omega_t, \omega_T, \omega_0)$ . The relation among  $\omega_t, \omega_T$  and  $\omega_0$  thus can be found experimentally. As we have stated previously that  $\omega_t = (\omega_0 \pm \nu) \mp \Omega$ , considering  $\nu$  as an arbitrary beating frequency and is substituted by  $\omega_T$ , we have  $\omega_t = (\omega_0 \pm \omega_T) \mp \Omega$ . This relation predicts that if several vibrational frequencies are coupled to a common frequency  $\Omega$ , in the  $A(\omega_t, \omega_T)$  map, the peak amplitude would be distributed along two groups of line characterized by a slope of “+1” and “-1” respectively, where “+1” stands for the coherence in the excited state and “-1” for the ground state, while the corresponding intercept equals to  $-\Omega$  and  $+\Omega$  respectively. The vibrational modes 80, 200, 280 cm<sup>-1</sup> in Fig. 3(b) are found to be coupled to the other modes. Therefore, it can be concluded that all these observed vibrational modes are coupled to one another constituting a wave-packet on the ground state and the excited-state potential surface respectively.

Then we employed TG measurement trying to identify the vibrational modes of BChla and BChla dimer in protein. Compared to 2DES, TG is a similar technique with the two pump pulses overlapped temporally hence having no resolution of the excitation wavelengths. Recently, quantitative fitting of the individual oscillation components have been reported for wave-packet dynamics [44], and damped oscillation in TA [45] and 2DES [46]. Singular value decomposition (SVD) method was employed to resolve the species-associated spectra and their corresponding decay kinetics (SI Fig. S6). The oscillation residual kinetics at every probe wave-

length was obtained by subtraction the by the globally fitted non-oscillating envelope (SI Fig. S7). Linear prediction singular value decomposition method was used to fit the oscillation frequencies with the equation  $A_\lambda(t) = \sum_{m=1}^N a_m \cos(\omega_m t + \phi_m) e^{-\gamma_m t}$  [47], where  $A_\lambda(t)$  denotes the oscillating residual kinetics at a given probing wavelength at  $\lambda$ ,  $m$  stands for a single oscillating component with an oscillating frequency  $\omega_m$ , an amplitude of  $a_m$ , an initial phase of  $\phi_m$  and a relaxation rate of  $\gamma_m$ . Based on the singular values of the SVD components, we set  $m = 35$ . Fig. 4 plots the fitted oscillation frequency along the probe wavelength for BChla (a) and B820 (b), as well as their oscillation frequency spectra (c) and (d) after summation of the intensity for a single oscillation frequency over all the probe wavelengths. Obviously, the distribution of the oscillation frequencies are more scattered for B820 than for BChla. The frequency distribution in Fig. 4(a) and (c) also support the coupled vibrational frequencies observed in 2DES.

We further compare the fitted oscillation frequencies and their corresponding decay time constants for BChla and B820 within a typical probe wavelength window, where the TG signals have the best signal-to-noise ratio. Fig. 5 plots the lifetime distribution of several vibrational frequencies within the selected probe window, and the results show that the protein scaffold does provide certain protection effect for the vibronic coherence. We noticed that, Kleinekathoer and coworkers have investigated theoretically the effect of protein on the long-lived coherences [48,49], and they shows that the protein induced fluctuations of the site energies does not play a role in long-lived coherences. However, our current case is different in that the excitation energy used is below that of the excitonic level (the excitonic splitting energy in B820 is 750 cm<sup>-1</sup> [13]), and the low energy vibronic coherence would not be mixed with that of the excitonic levels of BChla dimer.

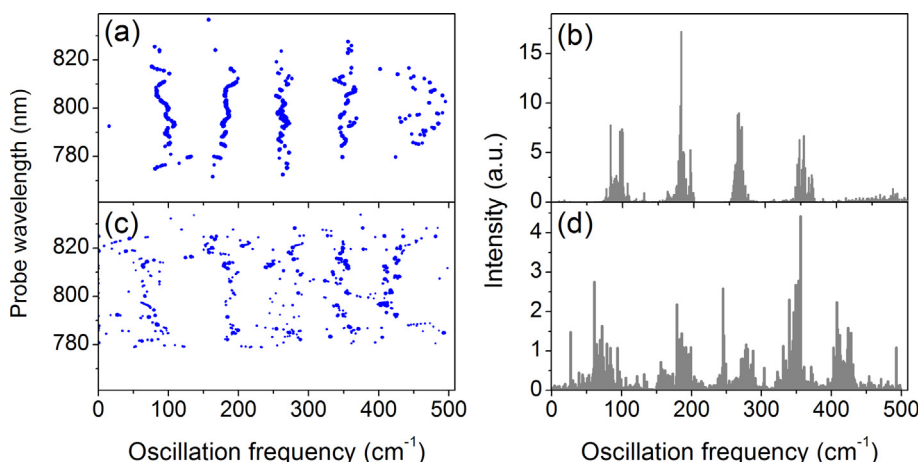


**Fig. 4.** LPSVD fitted oscillation frequency of the TG measured oscillation kinetics for BChla and B820. Fitted beating oscillation distribution along the probe wavelength for BChla (a) and B820 (c); frequency spectrum constructed by summed amplitude at a fitted oscillation frequency over all the probe wavelengths for BChla (b) and B820 (d).

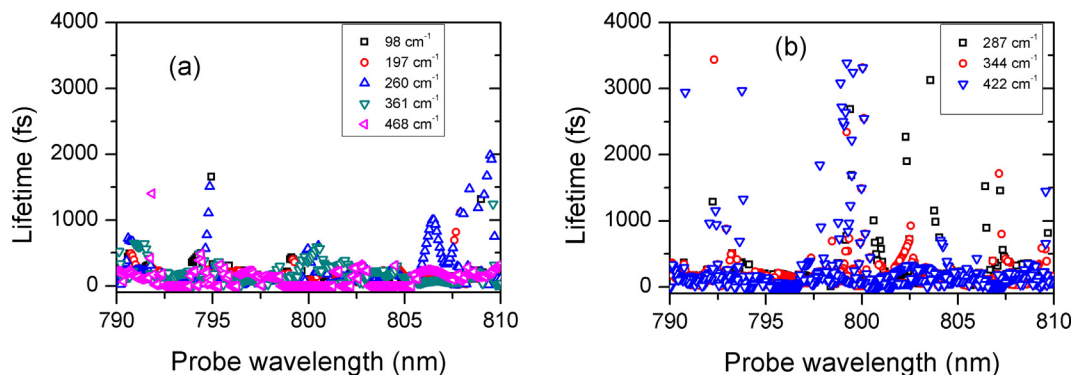


Fig. 5. Distribution of lifetime of several fitted oscillation frequencies within the selected probe window for BChla (a) and B820 (b).

#### 4. Conclusion

By investigation of the BChla in ethanol with 2DES and TG methods, beating dynamics have been observed. The corresponding frequencies retrieved by Fourier transformation of the beating dynamics are comparable to the reported values from RR spectra. The beating frequencies observed in 2DES are coupled and can be accounted by the proposed multi-vibrational mode coupled displaced oscillator model. By comparing the lifetimes for those low frequency modes observed in BChla monomer in ethanol with those for BChla dimer in B820 protein scaffold, we also find that the protein scaffold can protect the vibronic coherence which has not been mixed with that of the excitonic levels in the BChla dimer.

#### Acknowledgements

This work is supported by National Natural Science Foundation (NNSF) of China (Grant No. 21227003, 21433014).

#### Appendix A. Supplementary material

Supplementary data associated with this article can be found, in the online version, at <http://dx.doi.org/10.1016/j.cpllett.2017.03.029>.

#### References

- [1] R.E. Blankenship, *Molecular Mechanisms of Photosynthesis*, John Wiley & Sons, 2013.
- [2] E. Collini, Spectroscopic signatures of quantum-coherent energy transfer, *Chem. Soc. Rev.* 42 (2013) 4932–4947.
- [3] M.H. Vos, F. Rappaport, J.C. Lambry, J. Breton, J.L. Martin, Visualization of coherent nuclear motion in a membrane protein by femtosecond spectroscopy, *Nature* 363 (1993) 320–325.
- [4] M.H. Vos, M.R. Jones, C.N. Hunter, J. Breton, J.L. Martin, Coherent nuclear-dynamics at room-temperature in bacterial reaction centers, *Proc. Natl. Acad. Sci. USA* 91 (1994) 12701–12705.
- [5] G.S. Engel, T.R. Calhoun, E.L. Read, T.-K. Ahn, T. Mančal, Y.-C. Cheng, R.E. Blankenship, G.R. Fleming, Evidence for wavelike energy transfer through quantum coherence in photosynthetic systems, *Nature* 446 (2007) 782–786.
- [6] D.B. Turner, R. Dinshaw, K.K. Lee, M.S. Belsley, K.E. Wilk, P.M.G. Curmi, G.D. Scholes, Quantitative investigations of quantum coherence for a light-harvesting protein at conditions simulating photosynthesis, *Phys. Chem. Chem. Phys.* 14 (2012) 4857–4874.
- [7] G. Panitchayangkoon, D. Hayes, K.A. Fransted, J.R. Caram, E. Harel, J. Wen, R.E. Blankenship, G.S. Engel, Long-lived quantum coherence in photosynthetic complexes at physiological temperature, *Proc. Natl. Acad. Sci. USA* 107 (2010) 12766–12770.
- [8] E. Collini, C.Y. Wong, K.E. Wilk, P.M.G. Curmi, P. Brumer, G.D. Scholes, Coherently wired light-harvesting in photosynthetic marine algae at ambient temperature, *Nature* 463 (2010) 644–647.
- [9] E. Romero, R. Augulis, V.I. Novoderezhkin, M. Ferretti, J. Thieme, D. Zigmantas, R. van Grondelle, Quantum coherence in photosynthesis for efficient solar-energy conversion, *Nat. Phys.* 10 (2014) 676–682.
- [10] T.R. Calhoun, N.S. Ginsberg, G.S. Schlau-Cohen, Y.C. Cheng, M. Ballottari, R. Bassi, G.R. Fleming, Quantum coherence enabled determination of the energy

landscape in light-harvesting complex II, *J. Phys. Chem. B* 113 (2009) 16291–16295.

- [11] F. Novelli, A. Nazir, G.H. Richards, A. Roozbeh, K.E. Wilk, P.M. Curmi, J.A. Davis, Vibronic resonances facilitate excited-state coherence in light-harvesting proteins at room temperature, *J. Phys. Chem. Lett.* 6 (2015) 4573–4580.
- [12] M.L. Flanagan, P.D. Long, P.D. Dahlberg, B.S. Rolczynski, S.C. Massey, G.S. Engel, Mutations to R. sphaeroides reaction center perturb energy levels and vibronic coupling but not observed energy transfer rates, *J. Phys. Chem. A* 120 (2016) 1479–1487.
- [13] M. Ferretti, V.I. Novoderezhkin, E. Romero, R. Augulis, A. Pandit, D. Zigmantas, R. van Grondelle, The nature of coherences in the B820 bacteriochlorophyll dimer revealed by two-dimensional electronic spectroscopy, *Phys. Chem. Chem. Phys.* 16 (2014) 9930–9939.
- [14] P.C. Arpin, D.B. Turner, S.D. McClure, C.C. Jumper, T. Mirkovic, J.R. Challa, J. Lee, C.Y. Teng, B.R. Green, K.E. Wilk, P.M. Curmi, K. Hoef-Emden, D.W. McCamant, G.D. Scholes, Spectroscopic studies of cryptophyte light harvesting proteins: vibrations and coherent oscillations, *J. Phys. Chem. B* 119 (2015) 10025–10034.
- [15] E. Harel, G.S. Engel, Quantum coherence spectroscopy reveals complex dynamics in bacterial light-harvesting complex 2 (LH2), *Proc. Natl. Acad. Sci. USA* 109 (2012) 706–711.
- [16] F.D. Fuller, J. Pan, A. Gelzinis, V. Butkus, S.S. Senlik, D.E. Wilcox, C.F. Yocum, L. Valkunas, D. Abramavicius, Vibronic coherence in oxygenic photosynthesis, *J.P. Ogilvie, Nat. Chem.* 6 (2014) 706.
- [17] A. Ishizaki, G.R. Fleming, Theoretical examination of quantum coherence in a photosynthetic system at physiological temperature, *Proc. Natl. Acad. Sci. USA* 106 (2009) 17255–17260.
- [18] V. Perlik, C. Lincoln, F. Sanda, J. Hauer, Distinguishing electronic and vibronic coherence in 2D spectra by their temperature dependence, *J. Phys. Chem. Lett.* 5 (2014) 404–407.
- [19] A. Halpin, P.J. Johnson, R. Tempelaar, R.S. Murphy, J. Knoester, T.L. Jansen, R.J. Miller, Two-dimensional spectroscopy of a molecular dimer unveils the effects of vibronic coupling on exciton coherences, *Nat. Chem.* 6 (2014) 196–201.
- [20] V. Butkus, D. Zigmantas, L. Valkunas, D. Abramavicius, Vibrational vs. electronic coherences in 2D spectrum of molecular systems, *Chem. Phys. Lett.* 545 (2012) 40–43.
- [21] A.W. Chin, S.F. Huelga, M.B. Plenio, Coherence and decoherence in biological systems: principles of noise-assisted transport and the origin of long-lived coherences, *Phil. Trans. R. Soc. A* 370 (2012) 3638–3657.
- [22] N. Christensson, H.F. Kauffmann, T. Pullerits, T. Mancal, Origin of long-lived coherences in light-harvesting complexes, *J. Phys. Chem. B* 116 (2012) 7449–7454.
- [23] V. Tiwari, W.K. Peters, D.M. Jonas, Electronic resonance with anticorrelated pigment vibrations drives photosynthetic energy transfer outside the adiabatic framework, *Proc. Natl. Acad. Sci. USA* 110 (2013) 1203–1208.
- [24] A. Chenu, N. Christensson, H.F. Kauffmann, T. Mancal, Enhancement of vibronic and ground-state vibrational coherences in 2D spectra of photosynthetic complexes, *Sci. Rep.* 3 (2013) 2029.
- [25] F. Fassioli, A. Olaya-Castro, G.D. Scholes, Coherent energy transfer under incoherent light conditions, *J. Phys. Chem. Lett.* 3 (2012) 3136–3142.
- [26] H. Lee, Y.-C. Cheng, G.R. Fleming, Coherence dynamics in photosynthesis: protein protection of excitonic coherence, *Science* 316 (2007) 1462–1465.
- [27] K.R. Shelly, E.A. Carson, W.F. Beck, Vibrational coherence from the dipyrindine complex of bacteriochlorophyll a: intramolecular modes in the 10–220-cm<sup>-1</sup> regime, intermolecular solvent modes, and relevance to photosynthesis, *J. Am. Chem. Soc.* 125 (2003) 11810–11811.
- [28] V. Palaniappan, M.A. Aldema, H.A. Frank, D.F. Bocian, Qy-excitation resonance Raman scattering from the special pair in Rhodospirillum rubrum reaction centers. Implications for primary charge separation, *Biochemistry* 31 (1992) 11050–11058.
- [29] K. Czarniecki, J.R. Diers, V. Chynwat, J.P. Erickson, H.A. Frank, D.F. Bocian, Characterization of the strongly coupled, low-frequency vibrational modes of the special pair of photosynthetic reaction centers via isotopic labeling of the cofactors, *J. Am. Chem. Soc.* 119 (1997) 415–426.

- [30] A. Warshel, W.W. Parson, Spectroscopic properties of photosynthetic reaction centers. 1. Theory, *J. Am. Chem. Soc.* 109 (1987) 6143–6152.
- [31] W.W. Parson, A. Warshel, Spectroscopic properties of photosynthetic reaction centers. 2. Application of the theory to Rhodospseudomonas-viridis, *J. Am. Chem. Soc.* 109 (1987) 6152–6163.
- [32] S. Savikhin, W.S. Struve, Femtosecond pump-probe spectroscopy of bacteriochlorophyll *a* monomers in solution, *Biophys. J.* 67 (1994) 2002–2007.
- [33] M. Chachivili, H. Fidder, T. Pullerits, V. Sundstrom, Coherent nuclear motions in light-harvesting pigments and dye molecules, probed by ultrafast spectroscopy, *J. Raman Spectrosc.* 26 (1995) 513–522.
- [34] K.A. Fransted, J.R. Caram, D. Hayes, G.S. Engel, Two-dimensional electronic spectroscopy of bacteriochlorophyll *a* in solution: elucidating the coherence dynamics of the Fenna-Matthews-Olson complex using its chromophore as a control, *J. Chem. Phys.* 137 (2012) 125101.
- [35] S.S. Senlik, V.R. Policht, J.P. Ogilvie, Two-color nonlinear spectroscopy for the rapid acquisition of coherent dynamics, *J. Phys. Chem. Lett.* 6 (2015) 2413–2420.
- [36] J. Miller, S. Hinchigeri, P. Parkes-Loach, P. Callahan, J. Sprinkle, J. Riccobono, P. Loach, Isolation and characterization of a subunit form of the light-harvesting complex of Rhodospirillum rubrum, *Biochemistry* 26 (1987) 5055–5062.
- [37] T. Brixner, T. Mančal, I.V. Stiopkin, G.R. Fleming, Phase-stabilized two-dimensional electronic spectroscopy, *J. Chem. Phys.* 121 (2004) 4221–4236.
- [38] S. Yue, Z. Wang, X.-C. He, G.-B. Zhu, Y.-X. Weng, Construction of the apparatus for two dimensional electronic spectroscopy and characterization of the instrument, *Chin. J. Chem. Phys.* 28 (2015) 509–517.
- [39] F. Milota, C.N. Lincoln, J. Hauer, Precise phasing of 2D-electronic spectra in a fully non-collinear phase-matching geometry, *Opt. Express* 21 (2013) 15904–15911.
- [40] D. Egorova, Self-analysis of coherent oscillations in time-resolved optical signals, *J. Phys. Chem. A* 118 (2014) 10259–10267.
- [41] V. Butkus, L. Valkunas, D. Abramavicius, Vibronic phenomena and exciton-vibrational interference in two-dimensional spectra of molecular aggregates, *J. Chem. Phys.* 140 (2014) 034306.
- [42] E. Basinskaite, V. Butkus, D. Abramavicius, L. Valkunas, Vibronic models for nonlinear spectroscopy simulations, *Photosynth. Res.* 121 (2014) 95–106.
- [43] A.F. Fidler, G.S. Engel, Nonlinear spectroscopic theory of displaced harmonic oscillators with differing curvatures: a correlation function approach, *J. Phys. Chem. A* 117 (2013) 9444–9453.
- [44] S. Schott, L. Röss, J. Hrusak, P. Nuemberger, T. Brixner, Identification of photofragmentation patterns in trihalide anions by global analysis of vibrational wavepacket dynamics in broadband transient absorption data, *Phys. Chem. Chem. Phys.* 18 (2016) 33287–33302.
- [45] I.H.M. van Stokkum, C.C. Jumper, J.J. Snellenburg, G.D. Scholes, R. van Grondelle, P. Maly, Geometric phase effects in the ultracold H + H<sub>2</sub> reaction, *J. Chem. Phys.* 145 (2016) 164303.
- [46] A. Volpato, L. Bolzonello, E. Meneghin, E. Collini, Global analysis of coherence and population dynamics in 2D electronic spectroscopy, *Opt. Express* 24 (2016) 24773–24785.
- [47] R. Kumaresan, D.W. Tufts, Estimating the parameters of exponentially damped sinusoids and Pole-Zero modeling in noise, *IEEE Trans. Acoust. Speech Signal Process.* 30 (1982) 833–840.
- [48] C. Olbrich, J. Struempfer, K. Schulten, U. Kleinekathoefer, Quest for spatially correlated fluctuations in the FMO light-harvesting complex, *J. Phys. Chem. B* 115 (2011) 758–764.
- [49] C.P. van der Vegte, J.D. Prajapati, U. Kleinekathoefer, J. Knoester, T.L.C. Jansen, Atomistic modeling of two-dimensional electronic spectra and excited-state dynamics for a light harvesting 2 complex, *J. Phys. Chem. B* 119 (2015) 1302–1313.